



Cite this: DOI: 10.1039/c8dt02538j

# A solvent- and temperature-dependent intramolecular equilibrium of diamagnetic and paramagnetic states in Co complexes bearing triaryl amines†

Linda Schnaubelt,<sup>a</sup> Holm Petzold,<sup>b</sup> Evgenia Dmitrieva,<sup>b</sup> Marco Rosenkranz<sup>b</sup> and Heinrich Lang<sup>ID</sup> \*<sup>a</sup>

Complexes  $[\text{Co}(\text{L})_2](\text{ClO}_4)_2$  ( $\text{L} = o$ -substituted 2-(pyridine-2-yl)-1,10-phenanthrolines **1a–c**) containing three redox active centres (a  $\text{Co}^{2+}$  ion and two triaryl amine (Tara) units) have been synthesised. The order of oxidation steps in  $[\text{Co}(\text{L})_2](\text{ClO}_4)_2$  ( $\text{L} = \mathbf{1a–c}$ ) was determined using cyclic voltammetry and EPR/UV-vis-NIR spectroelectrochemistry. In acetonitrile solutions, at room temperature, the first oxidation is Co-centred followed by the Tara oxidation at more anodic potentials. The order of oxidation is inverted in solutions of the less polar solvent dichloromethane. The  $\text{Co}^{3+/2+}$ -centred redox event leads to a spin transition between the paramagnetic high-spin (HS)  $\text{Co}^{2+}$  and the diamagnetic low-spin (LS)  $\text{Co}^{3+}$  state, which was proven using  $^1\text{H}$  NMR and EPR spectroscopy. After one-electron oxidation of  $[\text{Co}(\text{L})_2](\text{ClO}_4)_2$ , an equilibrium between the diamagnetic  $[\text{Co}^{3+}(\text{L})]^{3+}$  and paramagnetic  $[\text{Co}^{2+}(\text{L})(\text{L}^+)]^{3+}$  state in  $[\text{Co}(\text{L})_2]^{3+}$  ( $\text{L} = \mathbf{1a–c}$ ) was found. Cyclic voltammetry showed enhanced intermolecular electron transfer between the  $[\text{Co}^{2+}(\text{L})_2]^{2+}$  and  $[\text{Co}^{3+}(\text{L})_2]^{3+}$  redox states mediated by  $[\text{Co}^{2+}(\text{L})(\text{L}^+)]^{3+}$ . Variable temperature vis-NIR spectroscopy of *in situ* generated  $[\text{Co}(\text{L})_2]^{3+}$  revealed a temperature-dependent redox equilibrium between the  $[\text{Co}^{3+}(\text{L})_2]^{3+}$  and the  $[\text{Co}^{2+}(\text{L})(\text{L}^+)]^{3+}$  states ( $\text{L} = \mathbf{1a–c}$ ). Magnetic coupling between the HS- $\text{Co}^{2+}$  ion and the Tara<sup>+</sup> radical in  $[\text{HS-Co}^{2+}(\text{L}^+)(\text{L})]^{3+}$  ( $\text{L} = \mathbf{1a,c}$ ) was deduced from broad and undetectable lines observed in the corresponding EPR spectra. Complete oxidation to  $[\text{LS-Co}^{3+}(\text{L}^+)_2]^{5+}$  ( $\text{L} = \mathbf{1a,c}$ ) leads to characteristic EPR spectra of Tara biradicals with non-interacting spins.

Received 21st June 2018,  
Accepted 21st August 2018

DOI: 10.1039/c8dt02538j

rsc.li/dalton

## Introduction

Metal complexes with multiple redox centres have gained interest, for example, in the development of sensors, electrochromic materials and memory storage media.<sup>1–4</sup> Intramolecular charge transfer (CT) between redox centres has been widely investigated on inorganic mixed-valence complexes with two metal redox centres.<sup>5–10</sup> Similarly, organic mixed-valence compounds<sup>11,12</sup> have attracted attention but hybrid organic/inorganic redox-active complexes have provoked a dynamic issue in CT research. Modulation of redox states and even spin multiplicities leads to characteristic changes in optical, magnetic and structural properties.<sup>13,14</sup>

Stimuli are most commonly a change in temperature and/or light-irradiation. In this context, polypyridine complexes of Ru,<sup>1–3,15–20</sup> Os<sup>21–24</sup> and Zn,<sup>25–29</sup> respectively, bearing triaryl amines (Taras) have attracted great attention, but less common are cobalt complexes.<sup>30,31</sup> The combination of redox-active cobalt ions and Taras in one molecule leads to hybrid materials with interesting properties such as enhanced light absorption,<sup>2,17</sup> electrochromism,<sup>18,32</sup> metal-to-ligand or ligand-to-metal charge transfer<sup>16,33</sup> (MLCT, LMCT) and spin transition. The LS- $\text{Co}^{3+}$ /HS- $\text{Co}^{2+}$  (LS = low spin, HS = high spin) redox couple has been an intriguing building block for charge transfer induced spin transition (CTIST) complexes.<sup>34–37</sup> Common examples are Prussian-blue analogues<sup>38,39</sup> and catecholate/semiquinone<sup>40–42</sup> systems. Their CTIST behaviour in the solid state has been investigated in detail but there is a lack of examination of the CTIST in solution.<sup>43,44</sup>

Recently, we reported on the synthesis, molecular structure and redox behaviour of  $[\text{Co}(\mathbf{1a})_2]^{2+}$ ,<sup>45</sup> possessing two phenanthroline-pyridyl based ligands which bear a redox-active Tara unit. Cyclic voltammetry and coupled EPR/UV-vis-NIR spectro-

<sup>a</sup>Technische Universität Chemnitz, Faculty of Natural Sciences, Institute of Chemistry, Inorganic Chemistry, 09107 Chemnitz, Germany.

E-mail: heinrich.lang@chemie.tu-chemnitz.de

<sup>b</sup>Center of Spectroelectrochemistry, Leibniz Institute for Solid State and Materials Research (IFW Dresden), Helmholtzstraße 20, 01069 Dresden, Germany

† Electronic supplementary information (ESI) available. See DOI: 10.1039/c8dt02538j

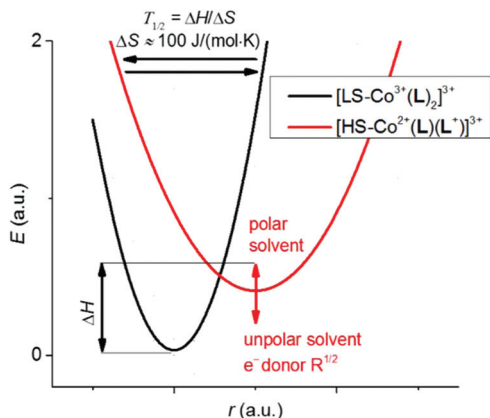


Fig. 1 Parabolic representation of the CTIST in complexes  $[\text{Co}(\text{L})_2]^{3+}$  ( $\text{L} = \mathbf{1a-c}$ ). LS = low-spin, HS = high-spin.

electrochemistry in acetonitrile evinced that the first oxidation process of  $[\text{Co}(\mathbf{1a})_2]^{2+}$  is Co-centred followed by the Tara-centred oxidation. The redox separation of the Co- and Tara-centred redox process in  $[\text{Co}(\mathbf{1a})_2]^{2+ \rightarrow 5+}$  amounts to  $\Delta E^{\circ} \approx 250$  mV. However, an equilibrium (Fig. 1) between the redox isomers  $[\text{Co}^{3+}(\mathbf{1a})_2]^{3+}$  and  $[\text{Co}^{2+}(\mathbf{1a})(\mathbf{1a}^+)]^{3+}$  was not directly observed. Co-centred redox events (reaction on the electrodes and self-exchange reaction) involving the LS-Co<sup>3+</sup>/HS-Co<sup>2+</sup> redox couple are mediated by the presence of the Tara unit, indicating the presence of paramagnetic  $[\text{Co}^{2+}(\mathbf{1a})(\mathbf{1a}^+)]^{3+}$  as a small fraction of the  $[\text{Co}(\mathbf{1a})_2]^{3+}$  redox state (parabolic representation in Fig. 1).

In search of complexes that are in a genuine equilibrium between the paramagnetic and diamagnetic state of  $[\text{Co}(\text{L})_2]^{3+}$ , we modified the *para*-substituents  $\text{R}^1$  and  $\text{R}^2$  of the Tara units. The variation of the Tara *para*-substituents is an efficient way of fine tuning its redox properties. Furthermore, enhanced intramolecular electron transfer in relation to small redox splitting ( $\Delta E^{\circ}$ ) of the donor and acceptor unit was

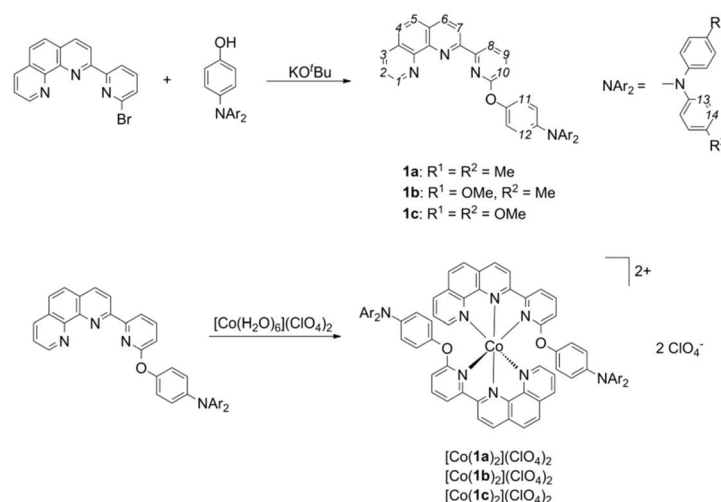
reported.<sup>46–48</sup> To decrease the redox separation between both redox sites, the Taras were alternated by introducing electron-rich methoxy groups. Substitution of a methyl group by a methoxy group reduces the redox potential of the Tara by approximately 70 mV.<sup>49</sup> Similarly, a difference in the solvent polarity can have a substantial effect on the redox potentials of the Co<sup>3+/2+</sup> and Tara<sup>+0</sup> couples.<sup>50</sup> Therefore, the redox behaviour of the complexes  $[\text{Co}(\text{L})_2](\text{ClO}_4)_2$  ( $\text{L} = \mathbf{1a-c}$ ) was investigated using cyclic voltammetry and coupled EPR/UV-vis-NIR spectroelectrochemistry in acetonitrile and dichloromethane. The results are supported by variable temperature (VT) NMR and vis-NIR spectroscopy of *in situ* oxidised  $[\text{Co}(\mathbf{1c})_2](\text{ClO}_4)_2$ .

## Results and discussion

### Synthesis and characterisation

Compounds  $\mathbf{1a-c}$  were synthesised from 2-(6-bromopyridine-2-yl)-1,10-phenanthroline<sup>45</sup> by a solvent-free melt reaction with an appropriate potassium salt of the respective *para*-hydroxyl-Tara (Tara = triaryl amine). The potassium salts of the hydroxyl-Taras were prepared in THF solution using KO<sup>t</sup>Bu. After removing all volatiles, 2-(6-bromopyridine-2-yl)-1,10-phenanthroline was added and the reaction mixture was heated until both components melted (>150 °C). Appropriate work-up and column chromatography afforded compounds  $\mathbf{1a-c}$  in moderate to good yields. The Co<sup>2+</sup> complexes were obtained after mixing  $\mathbf{1a-c}$  with  $[\text{Co}(\text{H}_2\text{O})_6](\text{ClO}_4)_2$  in ethanol solutions as air and moisture stable yellow solids. The synthesis methodologies are outlined in Scheme 1. All compounds were characterised using elemental analysis, mass spectrometry, and <sup>13</sup>C NMR (diamagnetic compounds only) and <sup>1</sup>H NMR spectroscopy. A detailed description of the synthesis and experimental data can be found in the ESI.†

<sup>1</sup>H NMR spectra of complexes  $[\text{Co}(\text{L})_2](\text{ClO}_4)_2$  ( $\text{L} = \mathbf{1a-c}$ ) in *d*<sub>3</sub>-acetonitrile reveal a paramagnetic behaviour caused by the *d*<sup>7</sup> high-spin configuration of the metal. At 298 K, proton reso-



Scheme 1 Synthesis of  $\mathbf{1a-c}$  and their corresponding  $\text{Co}^{2+}$  complexes  $[\text{Co}(\mathbf{1a-c})_2](\text{ClO}_4)_2$ . The small italic numbers indicate the proton labelling.

nances spread from about  $\delta = 170$  to  $-10$  ppm. Only the aromatic proton resonances of the tolyl and anisyl groups retain their doublet character ( $^3J_{\text{H,H}}$  coupling) due to the spatial distance to the paramagnetic  $\text{Co}^{2+}$  ion ( $1/r^6$  dependence of the relaxation enhancement). Short  $T_1$  relaxation times of the proton resonances are the result of dipolar coupling of the proton spins with the unpaired d-electrons of the cobalt ion ( $T_1 = 1\text{--}4$  ms for  $H1$ ). With regard to the intermediate ligand strength of *o*-substituted 2-(pyridine-2-yl)-1,10-phenanthrolines<sup>51,52</sup> and previously reported details on  $[\text{Co}(\mathbf{1a})_2]^{2+}$ ,<sup>45</sup> complexes  $[\text{Co}(\mathbf{L})_2](\text{ClO}_4)_2$  ( $\mathbf{L} = \mathbf{1a-c}$ ) are exclusively regarded as high-spin. The  $^1\text{H}$  NMR spectrum of  $[\text{Co}(\mathbf{1c})_2](\text{ClO}_4)_2$  at 198 K exhibits a strong paramagnetic shift of the 2-(pyridine-2-yl)-1,10-phenanthroline proton resonances to a lower field accompanied by substantial line broadening in accordance with the Curie behaviour and the increased solvent viscosity. The rotation of the phenyl rings with  $H11$  and  $H12$  is slowed down leading to additional line broadening for the resonances at  $\delta = -5.36$  and  $-16.56$  ppm (line widths = 396 and 600 Hz). Sub-stoichiometric oxidation of  $[\text{Co}(\mathbf{1c})_2]^{2+}$  to  $[\text{Co}(\mathbf{1c})_2]^{3+}$  with  $[\text{N}(p\text{-C}_6\text{H}_5\text{Br})_3][\text{SbCl}_6]$  leads to spreading out of all resonances at 298 K as a result of fast electron transfer between these two species (Fig. 15-SI†). Cooling  $d_6$ -acetone solutions down to 193 K decelerates the electron transfer and consequently the resonances sharpen for both  $[\text{Co}(\mathbf{1c})_2]^{2+}$  and  $[\text{Co}(\mathbf{1c})_2]^{3+}$ , respectively. Signals for the aromatic protons of  $[\text{Co}(\mathbf{1c})_2]^{3+}$  are observed between  $\delta = 10$  and 5.5 ppm revealing the diamagnetic LS- $\text{Co}^{3+}$  state. The assignment of the  $[\text{Co}^{3+}(\mathbf{1c})_2]^{3+}$  resonances was achieved by measuring the  $^1\text{H}, ^1\text{H}$  COSY spectrum and previously recorded EXSY spectra of related complexes.<sup>45</sup> In  $\text{Co}^{3+}$  polypyridyl complexes, the Co-N bond lengths are shorter than those in  $\text{Co}^{2+}$  polypyridyl species.<sup>53,54</sup> Hence, the rotation of the phenyl rings bearing  $H11$  and  $H12$  is hindered and two sets of resonances (four resonances in total) can be observed in the  $^1\text{H}$  NMR spectrum (Fig. 16-SI†).

## Electrochemistry

Complexes  $[\text{Co}(\mathbf{L})_2](\text{ClO}_4)_2$  ( $\mathbf{L} = \mathbf{1a-c}$ ) contain three redox-active centres, a  $\text{Co}^{2+}$  ion and two Tara units. Electrochemical studies are frequently employed to examine redox potentials and poss-

ible electronic coupling between the redox-active units. Thus, the redox behaviour of  $[\text{Co}(\mathbf{L})_2](\text{ClO}_4)_2$  ( $\mathbf{L} = \mathbf{1a-c}$ ) was studied using cyclic and square wave voltammetry. Cyclic voltammograms (CVs) and square wave voltammograms (SWVs) were recorded from anhydrous acetonitrile or dichloromethane solution of the respective complex (1 mM) with weakly coordinating  $[\text{tBu}_4\text{N}][\text{B}(\text{C}_6\text{F}_5)_4]$  (100 mM) as the supporting electrolyte<sup>55,56</sup> at 25 °C. All potentials were referenced to the ferrocene/ferrocenium ( $\text{FcH}/\text{FcH}^+$ ) redox couple.<sup>57</sup> Pertinent data are summarised in Table 1. Fig. 2 presents the corresponding CVs.

The CVs of complexes  $[\text{Co}(\mathbf{L})_2](\text{ClO}_4)_2$  ( $\mathbf{L} = \mathbf{1a-c}$ ) in acetonitrile solution exhibit two redox events. The first redox process can be assigned to the  $\text{Co}^{3+/2+}$  redox process followed by the Tara-centred redox process at higher potentials. The Tara groups are oxidised in a two-electron event consisting of two reversible superimposed redox waves. This indicates an insignificant electrostatic interaction between the two Taras, which is characteristic of distinct Tara nitrogen atoms.<sup>58,59</sup> The  $\text{Co}^{3+/2+}$  redox potentials remain constant with  $E^{\circ'}_1(\text{Co}^{3+/2+}) = 284, 290, 289$  mV in the series  $[\text{Co}(\mathbf{L})_2](\text{ClO}_4)_2$  ( $\mathbf{L} = \mathbf{1a-c}$ ). Usually, the  $\text{Co}^{3+/2+}$  redox process is characterised by large peak-to-peak separation due to large inner reorganis-

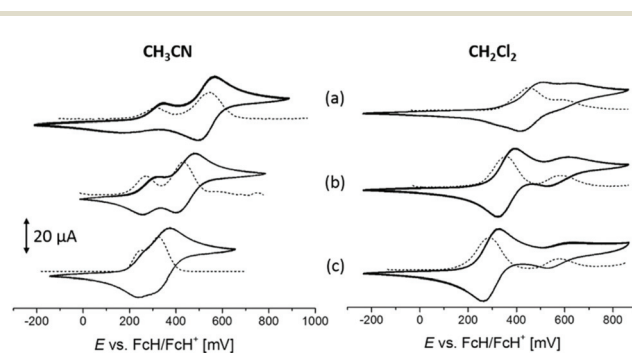


Fig. 2 Cyclic (solid) and square wave (dotted) voltammograms of (a)  $[\text{Co}(\mathbf{1a})_2](\text{ClO}_4)_2$ , (b)  $[\text{Co}(\mathbf{1b})_2](\text{ClO}_4)_2$  and (c)  $[\text{Co}(\mathbf{1c})_2](\text{ClO}_4)_2$  in  $\text{CH}_3\text{CN}$  (left) and in  $\text{CH}_2\text{Cl}_2$  (right). Measurement conditions: 1.0 mmol  $\text{L}^{-1}$  analyte,  $[\text{tBu}_4\text{N}][\text{B}(\text{C}_6\text{F}_5)_4]$  (0.1 mol  $\text{L}^{-1}$ ) as the supporting electrolyte, scan rates 100  $\text{mV s}^{-1}$  (CV) and 2  $\text{mV s}^{-1}$  (SWV), glassy carbon electrode, 25 °C.

Table 1 Cyclic voltammetry data of  $[\text{Co}(\mathbf{1a-c})_2](\text{ClO}_4)_2$  in  $\text{CH}_3\text{CN}$  and  $\text{CH}_2\text{Cl}_2$ .  $E^{\circ'}$  is the formal potential,  $\Delta E_p$  is the difference between the oxidation and reduction peak potentials, and  $\Delta E^{\circ'}$  is the difference between the  $\text{Co}^{3+/2+}$  and Tara $^{+/0}$  formal potentials. Measurement conditions: 1.0 mmol  $\text{L}^{-1}$  analyte,  $[\text{tBu}_4\text{N}][\text{B}(\text{C}_6\text{F}_5)_4]$  (0.1 mol  $\text{L}^{-1}$ ) as the supporting electrolyte, scan rate 100  $\text{mV s}^{-1}$ , glassy carbon electrode, 25 °C

Solvent $\text{CH}_3\text{CN}$	$E^{\circ'}_1(\text{Co}^{3+/2+})$ [mV]	$\Delta E_p(\text{Co}^{3+/2+})$ [mV]	$E^{\circ'}_2(\text{Tara}^{+/0})$ [mV]	$\Delta E_p(\text{Tara}^{+/0})$ [mV]	$\Delta E^{\circ'}$ [mV]
$[\text{Co}(\mathbf{1a})_2](\text{ClO}_4)_2$	284	106	531	68	247
$[\text{Co}(\mathbf{1b})_2](\text{ClO}_4)_2$	290	70	440	80	150
$[\text{Co}(\mathbf{1c})_2](\text{ClO}_4)_2$	289 <sup>a</sup>	60 <sup>a</sup>	374 <sup>a</sup>	90 <sup>a</sup>	85
Solvent $\text{CH}_2\text{Cl}_2$	$E^{\circ'}_1(\text{Tara}^{+/0})$ [mV]	$\Delta E_p(\text{Tara}^{+/0})$ [mV]	$E^{\circ'}_2(\text{Co}^{3+/2+})$ [mV]	$\Delta E_p(\text{Co}^{3+/2+})$ [mV]	$\Delta E^{\circ'}$ [mV]
$[\text{Co}(\mathbf{1a})_2](\text{ClO}_4)_2$	468 <sup>a</sup>	96 <sup>a</sup>	598 <sup>a</sup>	84 <sup>a</sup>	130
$[\text{Co}(\mathbf{1b})_2](\text{ClO}_4)_2$	364	74	578	90	214
$[\text{Co}(\mathbf{1c})_2](\text{ClO}_4)_2$	296	68	581	98	285

<sup>a</sup> Determined using square wave voltammetry.

ation.<sup>45,54,60</sup> So, noteworthy is the decrease in the peak-to-peak separation of the Co-centred redox process within the series of  $[\text{Co}(\text{L})_2](\text{ClO}_4)_2$  ( $\Delta E_p(\text{Co}^{3+/2+}) = 106$  ( $\text{L} = \mathbf{1a}$ ),  $70$  ( $\text{L} = \mathbf{1b}$ ), and  $60$  ( $\text{L} = \mathbf{1c}$ ) mV) concomitant with a smaller gap between the redox potentials of  $\text{Co}^{3+/2+}$  and  $\text{Tara}^{+/0}$ . This can be explained by the mediator effect of the Tara unit, which catalyses the  $\text{Co}^{3+/2+}$  redox process.<sup>45,61</sup> In this case, the Tara-centred oxidation to  $[\text{Co}^{2+}(\text{L})(\text{L}^+)]^{3+}$  is kinetically favoured due to the small inner reorganisation energy of the  $\text{Tara}^{+/0}$  redox couple. An intramolecular electron transfer leads to the thermodynamically more stable  $[\text{Co}^{3+}(\text{L})_2]^{3+}$  species.<sup>45</sup> The  $\text{Co}^{3+/2+}$  reduction peak in the CV of  $[\text{Co}(\mathbf{1a})_2](\text{ClO}_4)_2$  is sluggish. In contrast, this process is clearly visible in the CV of  $[\text{Co}(\mathbf{1b})_2](\text{ClO}_4)_2$ . The Tara-centred redox process is shifted cathodically from  $E^{\circ}_2(\text{Tara}^{+/0}) = 531$  mV in  $[\text{Co}(\mathbf{1a})_2](\text{ClO}_4)_2$  to  $E^{\circ}_2(\text{Tara}^{+/0}) = 440$  mV in  $[\text{Co}(\mathbf{1b})_2](\text{ClO}_4)_2$  and  $E^{\circ}_2(\text{Tara}^{+/0}) = 374$  mV in  $[\text{Co}(\mathbf{1c})_2](\text{ClO}_4)_2$ , due to the electron donor effect of the methoxy groups in the Tara units. The Co- and Tara-centred redox processes in  $[\text{Co}(\mathbf{1c})_2](\text{ClO}_4)_2$  are merged with a redox separation of  $\Delta E^{\circ} = 85$  mV. Therefore, SWV was used for the determination of the redox potentials. Cooling to  $-5$  °C leads to a cathodic shift of the redox potentials in  $[\text{Co}(\mathbf{1c})_2](\text{ClO}_4)_2$  ( $E^{\circ}_1(\text{Co}^{3+/2+}) = 210$  mV and  $E^{\circ}_2(\text{Tara}^{+/0}) = 320$  mV). The redox separation with  $\Delta E^{\circ} = 110$  mV has increased compared to the situation at  $25$  °C as a result of more facile formation of the  $[\text{Co}^{3+}(\text{L})_2]^{3+}$  species rather than  $[\text{Co}^{2+}(\text{L})(\text{L}^+)]^{3+}$  ( $\text{L} = \mathbf{1c}$ ) at lower temperatures (Fig. 1-SI†).

Redox processes are widely influenced by the solvents used. Polar solvents ( $\epsilon_r > 15$ ) are more capable of stabilising highly charged cations such as metal redox couples,  $\text{M}^{n+/m+}$  ( $m \neq 0$ ,  $n > m > +1$ ).<sup>50</sup> Neutral and singly charged cations such as organic radicals are less susceptible to such effects. In consequence we can expect a different response of potentials for the  $\text{Co}^{3+/2+}$  and  $\text{Tara}^{+/0}$  redox processes. A decrease in polarity of the solvent destabilises  $[\text{Co}^{3+}(\text{L})_2]^{3+}$  relative to the isomer structure  $[\text{Co}^{2+}(\text{L})(\text{L}^+)]^{3+}$  owing to the higher charge of the cobalt ion. Possibly an inversion of the order of redox processes can be achieved by variation of the solvent from  $\text{CH}_3\text{CN}$  ( $\epsilon_r = 35.9$ ) to  $\text{CH}_2\text{Cl}_2$  ( $\epsilon_r = 8.93$ ). The CVs and SWVs of  $[\text{Co}(\text{L})_2](\text{ClO}_4)_2$  ( $\text{L} = \mathbf{1a-c}$ ) were recorded in  $\text{CH}_2\text{Cl}_2$  under stationary measurement conditions.

The CVs of  $[\text{Co}(\text{L})_2](\text{ClO}_4)_2$  ( $\text{L} = \mathbf{1a-c}$ ) in  $\text{CH}_2\text{Cl}_2$  again exhibit two redox events, as discussed earlier (Fig. 2). However, compared to the situation in  $\text{CH}_3\text{CN}$ , the order of oxidation steps in  $\text{CH}_2\text{Cl}_2$  is inverted. The  $\text{Tara}^{+/0}$  redox events occur as two overlapping independent redox waves at  $E^{\circ}_1(\text{Tara}^{+/0}) = 468, 364, 296$  mV for  $[\text{Co}(\text{L})_2](\text{ClO}_4)_2$  ( $\text{L} = \mathbf{1a-c}$ ), which are cathodically shifted up to  $80$  mV relative to the  $\text{CH}_3\text{CN}$  solutions. The Tara redox process is followed by a  $\text{Co}^{3+/2+}$  redox event at higher potentials. The  $E^{\circ}$  values for the  $\text{Co}^{3+/2+}$  redox potentials in the series of  $[\text{Co}(\text{L})_2](\text{ClO}_4)_2$  ( $\text{L} = \mathbf{1a-c}$ ) are similar ( $E^{\circ}_2(\text{Co}^{3+/2+}) = 598, 578, 581$  mV). The Co-centred redox process is shifted anodically by  $\approx 300$  mV in comparison with  $\text{CH}_3\text{CN}$  solutions. The  $\text{Tara}^{+/0}$  and  $\text{Co}^{3+/2+}$  potential shifts verify the above mentioned influence of the solvent permittivities on differently charged species. The smallest redox separation in

dichloromethane solutions with  $\Delta E^{\circ} = 130$  mV is found for  $[\text{Co}(\mathbf{1a})_2](\text{ClO}_4)_2$ . The difference between the  $\text{Tara}^{+/0}$  and  $\text{Co}^{3+/2+}$  redox potentials increases in  $[\text{Co}(\text{L})_2](\text{ClO}_4)_2$  ( $\text{L} = \mathbf{1b,c}$ ) with the increasing electron donating character of the *para*-substituents at the Tara units ( $\Delta E^{\circ} = 214, 285$  mV).

### UV-vis-NIR spectroelectrochemistry

UV-vis-NIR spectra of  $[\text{Co}(\text{L})_2](\text{ClO}_4)_2$  ( $\text{L} = \mathbf{1a-c}$ ) exhibit one intense absorption around  $\lambda \approx 300$  nm both in  $\text{CH}_3\text{CN}$  and  $\text{CH}_2\text{Cl}_2$ . This absorption can be attributed to a  $\pi-\pi^*$  transition within the phenanthroline-pyridyl ligand and/or a Tara absorption.<sup>49,61-64</sup> The complexes are transparent at  $\lambda > 400$  nm. In contrast, the UV-vis-NIR spectra of  $\text{Co}^{3+}$ - and particularly  $\text{Tara}^+$ -centred transitions show characteristic absorptions. An absorption band related to the  $\text{Co}^{3+/2+}$  redox process of  $[\text{Co}^{3+/2+}(\mathbf{1a})_2]^{3+/2+}$  in  $\text{CH}_3\text{CN}$  was observed at  $\lambda = 382$  nm.<sup>45</sup> The  $\text{Tara}^+$ -centred transitions of  $[\text{Co}^{3+}(\mathbf{1a})_2]^{5+}$  appeared at  $\lambda = 682$  nm with a shoulder at  $\lambda = 558$  nm and a higher energy transition at  $\lambda = 365$  nm.<sup>45</sup> These are characteristic absorptions for Tara radicals.<sup>49,61</sup> To verify these statements UV-vis-NIR spectroelectrochemistry measurements of  $[\text{Co}(\text{L})_2](\text{ClO}_4)_2$  ( $\text{L} = \mathbf{1a-c}$ ) (2 mM) were carried out in anhydrous  $\text{CH}_3\text{CN}$  and  $\text{CH}_2\text{Cl}_2$ , respectively, using an OTTLE<sup>65</sup> cell (optically transparent thin-layer electrochemistry cell, quartz windows) with  $[\text{Bu}_4\text{N}][\text{B}(\text{C}_6\text{F}_5)_4]$  (0.1 M) as the supporting electrolyte at  $25$  °C.

An absorption band related to the  $\text{Co}^{3+/2+}$  redox process appears at  $\lambda_{\text{max}} = 382, 379, 380$  nm for complexes  $[\text{Co}^{3+}(\text{L})_2]^{3+}$  ( $\text{L} = \mathbf{1a-c}$ ) in  $\text{CH}_3\text{CN}$  solutions. This transition was verified using EPR/UV-vis-NIR spectroelectrochemistry measurements (*vide infra*) and appears at lower potentials than the  $\text{Tara}^+$ -related absorption bands in  $[\text{Co}(\text{L})_2](\text{ClO}_4)_2$  ( $\text{L} = \mathbf{1a,b}$ ) (Fig. 2 and 3-SI†). For  $[\text{Co}(\mathbf{1c})_2](\text{ClO}_4)_2$  a concomitant growth of the  $\text{Co}^{3+/2+}$  transition and  $\text{Tara}^+$  absorptions is observed (Fig. 4-SI†). The  $\text{Tara}^+$  absorption of  $[\text{Co}^{3+}(\text{L})_2]^{5+}$  ( $\text{L} = \mathbf{1a-c}$ ) appears at  $\lambda_{\text{max}} = 682, 720, 753$  nm in  $\text{CH}_3\text{CN}$  as intense bands ( $\epsilon_{\text{max}} = 25\,000-50\,000$  L mol<sup>-1</sup> cm<sup>-1</sup>) accompanied by a weaker shoulder between  $\lambda = 450$  and  $600$  nm and a higher energy transition at  $\lambda = 365, 362$  and  $363$  nm. A bathochromic shift of the absorption in the vis-region is observed with an increasing M-donor effect of the  $\text{Tara}^+$  substituents  $R^{1/2}$  within the series of  $[\text{Co}^{3+}(\text{L})_2]^{5+}$  ( $\text{L} = \mathbf{1a-c}$ ). This tendency is also observed for the  $\text{Tara}^+$  transition in  $\text{CH}_2\text{Cl}_2$  solutions ( $\lambda_{\text{max}} = 698, 736, 778$  nm for  $[\text{Co}^{3+/2+}(\text{L})_2]^{5+/4+}$  ( $\text{L} = \mathbf{1a-c}$ )). The higher energy transition of  $\text{Tara}^+$  in  $\text{CH}_2\text{Cl}_2$  is shifted around  $10-16$  nm to  $\lambda_{\text{max}} = 349, 352, 353$  nm for  $[\text{Co}^{3+/2+}(\text{L})_2]^{5+/4+}$  ( $\text{L} = \mathbf{1a-c}$ ) compared to the situation in  $\text{CH}_3\text{CN}$ . A transition which is connected to the  $\text{Co}^{3+/2+}$  redox process was found at  $\lambda_{\text{max}} = 369, 368, 366$  nm for  $[\text{Co}^{3+/2+}(\text{L})_2]^{5+/4+}$  ( $\text{L} = \mathbf{1a-c}$ ) in  $\text{CH}_2\text{Cl}_2$ . Its intensity is smaller with respect to the measurements in  $\text{CH}_3\text{CN}$  solutions, possibly due to the spin interaction (*vide infra*). Charge transfer bands, assignable to a direct electron transfer between the Co and Tara redox centres in their oxidised or reduced state, cannot be observed in both solvents. This is mainly caused by the large distance ( $d \approx 8.4$  Å)<sup>45</sup> between the two redox centres and the consequent weak electronic coupling. Similarly, indication for an ICVT charge trans-

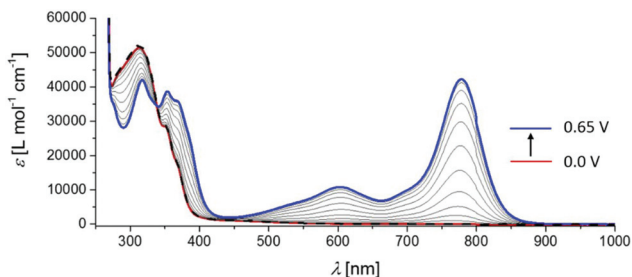


**Fig. 3** UV-vis-NIR spectra of  $[\text{Co}(\mathbf{1c})_2](\text{ClO}_4)_2$  at rising potentials vs. Ag/AgCl in  $\text{CH}_2\text{Cl}_2$ . The black dashed line is recorded after a series of oxidation measurements at  $-0.3$  V to prove the reversibility. Measurement conditions:  $2.0$  mmol  $\text{L}^{-1}$  analyte,  $[\text{t}^{\text{Bu}}_4\text{N}][\text{B}(\text{C}_6\text{F}_5)_4]$  ( $0.1$  M) as the supporting electrolyte,  $25$  °C.

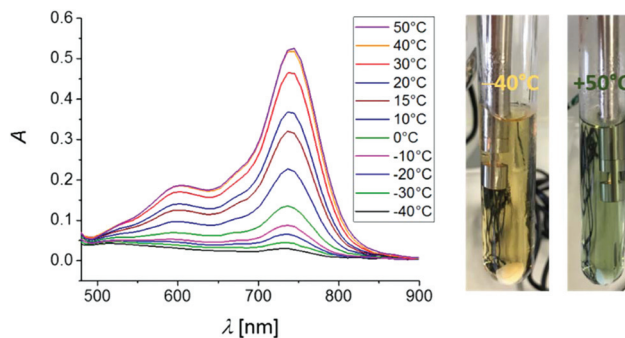


**Fig. 4** [left] VT vis-NIR spectra of  $[\text{Co}(\mathbf{1c})_2](\text{ClO}_4)_2$  which is partly oxidised to  $[\text{Co}(\mathbf{1c})_2]^{3+}$  using 1 eq. of  $[\text{N}(p\text{-C}_6\text{H}_5\text{Br})_3][\text{SbCl}_6]$  in  $\text{CH}_3\text{CN}$ . [right] Examined solution of  $[\text{Co}(\mathbf{1c})_2]^{3+}$  in  $\text{CH}_3\text{CN}$  at  $-40$  °C and  $+50$  °C. The colour changes from yellow ( $[\text{Co}^{3+}(\mathbf{1c})_2]^{3+}$ ) to green ( $[\text{Co}^{2+}(\mathbf{1c}^+)]^{3+}$ ).

fer band assignable to charge transfer between Tara and Tara<sup>+</sup> in  $[\text{Co}^{3+}(\mathbf{L})(\mathbf{L}^+)]^{4+}$  redox states is not found.<sup>59</sup> All oxidations from  $[\text{Co}^{2+}(\mathbf{L})_2]^{2+}$  to  $[\text{Co}^{3+}(\mathbf{L})_2]^{5+}$  ( $\mathbf{L} = \mathbf{1a-c}$ ) were reversible, which was proven by recording an additional spectrum after reduction at  $-0.3$  V (Fig. 3).

### VT vis-NIR spectroscopy

The CVs of  $[\text{Co}(\mathbf{1c})_2](\text{ClO}_4)_2$  in  $\text{CH}_3\text{CN}$  indicated a difference between the Co- and Tara-centred redox potentials of only  $\Delta E^{\circ} = 85$  mV. However, electronic communication between Co and Tara is too weak to be detected in the UV-vis-NIR spectroelectrochemical measurements for the *in situ* generated  $[\text{Co}(\mathbf{1c})_2]^{3+}$  species. Previous VT <sup>1</sup>H NMR (VT = variable temperature) spectroscopic measurements on partly oxidised  $[\text{Co}(\mathbf{1a})_2](\text{ClO}_4)_2$  revealed an accelerated self-exchange of the  $\text{Co}^{3+/2+}$  redox couple in comparison with  $\text{Co}^{3+/2+}$  complexes without a redox mediator.<sup>45</sup> This self-exchange can be frozen out at low temperatures. Such behaviour was also found for partly oxidised  $[\text{Co}(\mathbf{1c})_2](\text{ClO}_4)_2$  (*vide supra*). Apart from the kinetic effect, redox equilibria involving the  $\text{Co}^{3+/2+}$  redox couple are often strongly temperature dependent. This thermodynamic effect is a consequence of the large entropy difference between HS- $\text{Co}^{2+}$  and LS- $\text{Co}^{3+}$  ( $\approx 100$  J mol<sup>-1</sup> K<sup>-1</sup>).<sup>41,66,67</sup> A temperature dependent shift of the equilibrium between the  $[\text{Co}^{2+}(\mathbf{L})(\mathbf{L})]^{3+}$  and  $[\text{Co}^{3+}(\mathbf{L})_2]^{3+}$  states must exhibit characteristic changes of the absorption in the vis-NIR region. Therefore,  $[\text{Co}(\mathbf{1c})_2](\text{ClO}_4)_2$  was partly oxidised to  $[\text{Co}(\mathbf{1c})_2]^{3+}$  using 1 eq. of  $[\text{N}(p\text{-C}_6\text{H}_5\text{Br})_3][\text{SbCl}_6]$  (“magic blue”) in  $\text{CH}_3\text{CN}$ . From this solution vis-NIR spectra were recorded in the temperature range of  $-40$  °C and  $+50$  °C. The reduced oxidant, tris (4-bromophenyl)amine shows no vis-NIR absorption.<sup>59</sup> The spectra are depicted in Fig. 4 and show the obvious thermo-chromic behaviour of the solutions. The yellow colour and the absence of any absorptions in the range of 500–900 nm indicate the preference of the  $[\text{Co}^{3+}(\mathbf{1c})_2]^{3+}$  species at  $-40$  °C. With increasing temperature the colour changes from yellow ( $-40$  °C) to green ( $+50$  °C). An absorption band at  $\lambda_{\text{max}} = 745$  nm arises, which is characteristic of Tara<sup>+</sup> radicals (*vide supra*) and is associated with the formation of the  $[\text{Co}^{2+}(\mathbf{1c}^+)]^{3+}$  species. This is also in line with entropy-driven spin

transition reactions, having the maximum possible number of unpaired electrons with increasing temperature.<sup>68–71</sup> A similar temperature dependent equilibrium between the  $\text{Co}^{2+}$ /Tara<sup>+</sup> and  $\text{Co}^{3+}$ /Tara states was observed for  $[\text{Co}(\mathbf{1a})_2]^{3+}$  in  $\text{CH}_2\text{Cl}_2$  (Fig. 8-SI†). At ambient temperature, the Tara oxidation occurs 130 mV prior to the Co-centred oxidation; thus, addition of 1 eq. of “magic blue” to  $[\text{Co}^{2+}(\mathbf{1a})_2]^{2+}$  leads to the formation of the blue coloured  $[\text{Co}^{2+}(\mathbf{1a}^+)(\mathbf{1a})]^{3+}$  complex in  $\text{CH}_2\text{Cl}_2$  at  $T = 23$  °C. The absorption spectrum shows a characteristic band at  $\lambda_{\text{max}} = 685$  nm with a weaker shoulder. Cooling to  $T = -90$  °C leads to the formation of the yellow coloured  $[\text{Co}^{3+}(\mathbf{1a})_2]^{3+}$  species and consequently, to a significant decrease in the absorption band at  $\lambda_{\text{max}} = 685$  nm.

### EPR/UV-vis-NIR spectroelectrochemistry

For verification of the above statements in the oxidation order of complexes  $[\text{Co}(\mathbf{L})_2](\text{ClO}_4)_2$  ( $\mathbf{L} = \mathbf{1a,c}$ ), coupled EPR/UV-vis-NIR (electron paramagnetic resonance/ultraviolet-visible-near infrared) spectroelectrochemistry experiments were conducted. Tara radical and Tara biradical cations with non-interacting spins exhibit characteristic temperature-dependent EPR line-shapes.<sup>59</sup> The HS- $\text{Co}^{2+}$  ion is EPR-active but as a result of its fast electron relaxation ( $S = 3/2$ ), only broad lines are observed at  $T > 20$  K.<sup>72,73</sup> In contrast, the LS- $\text{Co}^{3+}$  ion is EPR silent due to its diamagnetic behaviour. Thus it is expected that valid EPR spectra are limited to *in situ* generated radicals  $[\text{Co}^{2+}(\mathbf{L})(\mathbf{L}^+)]^{3+}$  and  $[\text{Co}^{3+}(\mathbf{L})(\mathbf{L}^+)]^{4+}$ , and biradical complexes  $[\text{Co}^{3+}(\mathbf{L})_2]^{5+}$  and  $[\text{Co}^{2+}(\mathbf{L})_2]^{4+}$  ( $\mathbf{L} = \mathbf{1a,c}$ ). Increased electron relaxation caused by dipolar magnetic coupling between the  $\text{Co}^{2+}$  magnetic moment and the Tara<sup>+</sup> radical further restricts the EPR observable species to the  $\text{Co}^{3+}$  state, namely the  $[\text{Co}^{3+}(\mathbf{L})(\mathbf{L}^+)]^{4+}$  and  $[\text{Co}^{3+}(\mathbf{L})_2]^{5+}$  species. The measurements were carried out with an X-band CW spectrometer (microwave power of 5 mW, 100 kHz modulation) at 25 °C. The analyte dissolved in anhydrous  $\text{CH}_3\text{CN}$  or  $\text{CH}_2\text{Cl}_2$  with 0.1 M  $[\text{t}^{\text{Bu}}_4\text{N}][\text{B}(\text{C}_6\text{F}_5)_4]$  as the supporting electrolyte was placed in an optical EPR cavity.

*In situ* oxidation of  $[\text{Co}^{2+}(\mathbf{1a})_2]^{2+}$  to  $[\text{Co}^{3+}(\mathbf{1a})_2]^{3+}$  in  $\text{CH}_3\text{CN}$  leads to an increase of an absorption band at  $\lambda = 378$  nm

(Fig. 9-SI†). Thus this band is a marker for the  $\text{Co}^{3+/2+}$ -related redox event; at the same time, EPR spectra remain featureless. Upon further increase of the oxidation potential an EPR signal appears with a simultaneously rising absorption band at  $\lambda = 682$  nm. This feature indicates the *in situ* formation of the  $[\text{Co}^{3+}(\mathbf{1a})(\mathbf{1a}^+)]^{4+}$  and/or  $[\text{Co}^{3+}(\mathbf{1a})_2]^{5+}$  species. The  $g$  value amounts to 2.0031, close to the value of a free electron, which is characteristic of triphenyl amine radicals.<sup>59,74</sup>

The CV in  $\text{CH}_3\text{CN}$  for  $[\text{Co}(\mathbf{1c})_2](\text{ClO}_4)_2$  exhibits two overlapping redox processes; this is also reflected by simultaneously rising absorption bands in the UV-vis-NIR spectra for the Co- and Tara-centred oxidation ( $\lambda_{\text{max}}(\text{Co}^{3+}) = 380$  nm and  $\lambda_{\text{max}}(\text{Tara}^+) = 599/748$  nm). Hence, in  $\text{CH}_3\text{CN}$  solution  $[\text{Co}(\mathbf{1c})_2]^{3+}$  is found in a genuine equilibrium between  $[\text{Co}^{3+}(\mathbf{1c})_2]^{3+}$  and  $[\text{Co}^{2+}(\mathbf{1c})(\mathbf{1c}^+)]^{3+}$ . With the *in situ* formation of  $[\text{Co}^{3+}(\mathbf{1c})_2]^{5+}$  an EPR signal with a five line pattern appears with a  $g$  value of 2.0032. In contrast to  $[\text{Co}(\mathbf{1a})_2](\text{ClO}_4)_2$ , for the methoxy-substituted complex  $[\text{Co}(\mathbf{1c})_2](\text{ClO}_4)_2$  the potential dependence of the EPR intensity does not match the potential dependence of the  $\text{Tara}^+$  absorption band intensity (Fig. 11-SI† bottom left). The EPR signal appears at higher potentials than the  $\text{Tara}^+$  absorptions. It increases by further oxidation, while the absorptions reach a plateau. This can be explained by electron spin exchange between  $\text{HS-Co}^{2+}$  and  $\text{Tara}^+$  due to overlapping redox processes (*vide infra*). To obtain a better resolved line shape the EPR measurement for  $[\text{Co}^{3+}(\mathbf{1c})_2]^{5+}$  was repeated at  $T = 100$  K (Fig. 12-SI†). The  $g$  factor is anisotropic with  $g_1 = 2.0155$ ,  $g_2 = 2.0029$  and  $g_3 = 1.9898$ . Additionally, an EPR signal could not be detected at half-field, indicating no interaction between the two  $\text{Tara}^+$  spin centres ( $d \approx 14$  Å).<sup>75,76</sup>

In  $\text{CH}_2\text{Cl}_2$  solutions, the Co- and Tara-centred redox processes of  $[\text{Co}(\mathbf{1a})_2](\text{ClO}_4)_2$  are merged (*vide supra*), which is reflected by the plot of the potential dependence of the absorption of characteristic UV bands and the EPR detected spin density obtained from combined EPR/UV-vis-NIR spectroelectrochemical experiments (Fig. 10-SI†). At  $E = 0.5$  V complex  $[\text{Co}(\mathbf{1a})_2]^{2+}$  is partly oxidised, and only a weak and broad EPR signal is detected. A quantitative model for the complicated equilibria between the different redox states involved in the successive oxidation cannot be derived. However, UV-vis markers indicating the presence of  $\text{Tara}^+$  radicals increase slightly before the EPR detected spin density. This finding is consistent with a dominant first oxidation of  $[\text{Co}^{2+}(\mathbf{1a})_2]^{2+}$  to the  $\text{Tara}^+$  radical  $[\text{Co}^{2+}(\mathbf{1a})(\mathbf{1a}^+)]^{3+}$ . The latter shows no EPR response (under the experimental conditions used) due to dipolar coupling to the  $\text{HS-Co}^{2+}$ . A simultaneous formation of the EPR silent  $[\text{Co}^{3+}(\mathbf{1a})_2]^{3+}$  with a weak marker band for  $\text{Co}^{3+}$  in  $\text{CH}_2\text{Cl}_2$  cannot be ruled out. The first oxidation step is immediately followed by the oxidation to the EPR active  $\text{Tara}^+$  radical  $[\text{Co}^{3+}(\mathbf{1a})(\mathbf{1a}^+)]^{4+}$  and/or biradical  $[\text{Co}^{3+}(\mathbf{1a})_2]^{5+}$ . The EPR signal with significant higher intensity appears at  $E = 0.85$  V with  $g = 2.0037$ .

The case of  $[\text{Co}(\mathbf{1c})_2]^{3+}$  in  $\text{CH}_2\text{Cl}_2$  solution is the antipode to  $[\text{Co}(\mathbf{1a})_2]^{3+}$  in  $\text{CH}_3\text{CN}$ . The CV measurements revealed a Tara-centred oxidation occurring 285 mV prior to the Co-centred oxidation. During the first oxidation step  $[\text{Co}^{2+}(\mathbf{1c})(\mathbf{1c}^+)]^{3+}$  and  $[\text{Co}^{2+}(\mathbf{1c})_2]^{4+}$  complexes are formed. Both complexes contain  $\text{Tara}^+$  units but only a broad and small 3-line EPR signal is detected in  $\text{CH}_2\text{Cl}_2$  at  $E = 0.5$  V (Fig. 5). Dipolar coupling to the  $\text{HS-Co}^{2+}$  ion and collisions in solution between paramagnetic

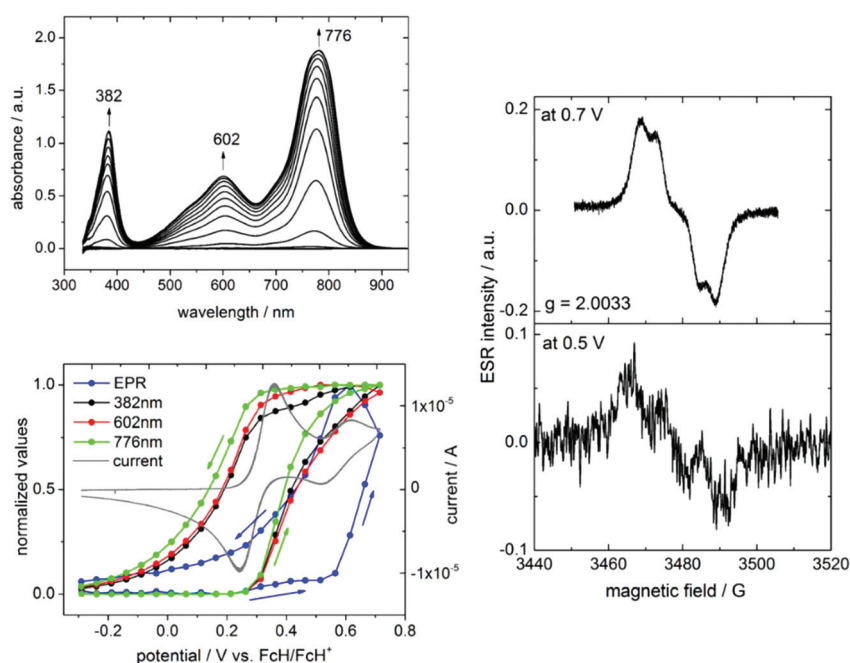


Fig. 5 [top left] *In situ* absorption spectra of  $[\text{Co}(\mathbf{1c})_2](\text{ClO}_4)_2$  in  $\text{CH}_2\text{Cl}_2$ . [bottom left] Potential dependence of the absorption bands and EPR intensity. [right] EPR spectra recorded at  $E = 0.5$  V ( $[\text{Co}^{2+}(\mathbf{1c})_2]^{4+}$ ) and  $E = 0.7$  V ( $[\text{Co}^{3+}(\mathbf{1c})_2]^{5+}$ ) at  $T = 298$  K.

metal ions and organic radicals cause broadening of the organic radical EPR signal.<sup>73,77,78</sup> The interaction leads to an electron–spin exchange and “transfer” of the short relaxation times of the HS-Co<sup>2+</sup> ions to the Tara<sup>+</sup> spins. This behaviour is immediately quenched by the oxidation of the paramagnetic Co<sup>2+</sup> ion to diamagnetic Co<sup>3+</sup> ( $E = 0.7$  V) resulting in an intense EPR signal for the [Co<sup>3+</sup>(**1c**<sup>+</sup>)<sub>2</sub>]<sup>5+</sup> species ( $g = 2.0033$ ) with a hyperfine splitting (triplet). The intensity of the EPR signal drops immediately when [Co<sup>3+</sup>(**1c**<sup>+</sup>)<sub>2</sub>]<sup>5+</sup> is reduced to [Co<sup>2+</sup>(**1c**<sup>+</sup>)<sub>2</sub>]<sup>4+</sup> in the reverse scan. The dipolar coupling between Tara<sup>+</sup> and HS-Co<sup>2+</sup> was also observed for [Co(**1a**)<sub>2</sub>](ClO<sub>4</sub>)<sub>2</sub> in CH<sub>2</sub>Cl<sub>2</sub> and [Co(**1c**)<sub>2</sub>](ClO<sub>4</sub>)<sub>2</sub> in CH<sub>3</sub>CN, but in less extent.

## Conclusions

Herein, a series of [Co<sup>2+</sup>(L)<sub>2</sub>]<sup>2+</sup> (L = **1a–c**) complexes is presented. The complexes have three redox-active sites that can be oxidised to form the tri-, tetra- and penta-cationic analogues. Particularly in solution, the tri- and tetra-cationic complexes [Co(L)<sub>2</sub>]<sup>3+</sup> and [Co(L)<sub>2</sub>]<sup>4+</sup> (L = **1a–c**) exist in an equilibrium state of different redox isomers. Depending on the solvent and the temperature either the HS-Co<sup>2+</sup> ion is oxidised to the LS-Co<sup>3+</sup> ion (HS = high-spin, LS = low-spin) or the Tara substituents are oxidised to the Tara<sup>+</sup> radical. This equilibrium, *e.g.* between [Co<sup>2+</sup>(L)(L<sup>+</sup>)]<sup>3+</sup> and [Co<sup>3+</sup>(L)<sub>2</sub>]<sup>3+</sup>, is strongly temperature and solvent dependent. In CH<sub>3</sub>CN, the Co<sup>2+</sup> oxidation occurs at lower potentials than the Tara oxidation. The oxidation order is reversed in CH<sub>2</sub>Cl<sub>2</sub>, due to different solvation energies. The equilibrium involves two species with different spin multiplicities (*e.g.*  $S = 0$  and  $S = 2$ ) representing a CTIST equilibrium (CTIST = charge transfer induced spin transition). Together with the different absorptions of the Tara and Tara<sup>+</sup> radicals thermochromic and solvatochromic behaviours are observed for [Co(L)<sub>2</sub>]<sup>3+</sup> (L = **1a–c**). Coupled EPR/spectroelectrochemical measurements proved the existence of this equilibrium. Moreover, characteristic absorption bands in the UV-vis-NIR as well as the pattern in the EPR spectra served as indicators for the equilibrium position. VT <sup>1</sup>H NMR spectroscopy and VT vis-NIR spectroscopy further verified these findings. The solvatochromic behaviour was ascribed to the different solvation energies of the Co<sup>3+/2+</sup> and Tara<sup>+/0</sup> redox couples. The thermochromic behaviour is the consequence of the strongly different entropies of the redox isomers. In summary, the complexes [Co(L)<sub>2</sub>]<sup>3+/4+</sup> represent interesting building blocks for the construction of molecular switches.

## Experimental

### General remarks

All reactions handling sensitive chemicals were carried out under an atmosphere of argon using standard Schlenk and cannula techniques. Anhydrous ethanol was purchased commercially from Acros Organics. Toluene was obtained from a

solvent purification system SPS-800 by MBraun. Tetrahydrofuran was purified by distillation from sodium/benzophenone ketyl. 2-(6-Bromopyridin-2-yl)-1,10-phenanthroline, **1a** and [Co(**1a**)<sub>2</sub>](ClO<sub>4</sub>)<sub>2</sub> were synthesised as previously reported in the literature.<sup>45</sup> The synthesis of employed triaryl amines is described in the ESI.† All other chemicals were purchased from commercial suppliers and were used without further purification.

NMR spectra were recorded with a Bruker Avance III 500 spectrometer; chemical shifts for <sup>1</sup>H and <sup>13</sup>C NMR are referenced internally to the residual protons and to the <sup>13</sup>C NMR signal of the deuterated solvent. Elemental analyses were performed using a Thermo FlashAE 1112 analyser. Mass spectra were recorded with a Bruker micrOTOF-QIIa mass spectrometer operating in the ESI mode (ESI = electrospray ionisation).

### Synthetic procedure

4-((6-(1,10-Phenanthrolin-2-yl)pyridin-2-yl)oxy)-N-(4-methoxyphenyl)-N-(*p*-tolyl)aniline (**1b**). 410 mg (1.34 mmol) of 4-((4-methoxyphenyl)(*p*-tolyl)amino)phenol and 126 mg (1.12 mmol) of potassium *tert*-butoxide were dissolved in 3 mL of anhydrous THF and heated to 60 °C for 2 h. After removing all volatile materials under vacuum, 264 mg (0.78 mmol) of 2-(6-bromopyridin-2-yl)-1,10-phenanthroline were added in a single portion. The respective reaction mixture was heated to 200 °C overnight. The molten material was cooled down to ambient temperature and was then dissolved in 20 mL of CH<sub>2</sub>Cl<sub>2</sub> and extracted twice with an aqueous NaHCO<sub>3</sub> solution. The organic phase was dried over Na<sub>2</sub>SO<sub>4</sub> and all volatiles were removed under vacuum. The crude product was purified *via* column chromatography over ALOX (column size: 2.5 × 20 cm) with a mixture of *n*-hexane/CH<sub>2</sub>Cl<sub>2</sub> (1 : 1; v/v) and 3% NEt<sub>3</sub> as the eluent. Yield: 110 mg, yellow solid (25% based on 2-(6-bromopyridin-2-yl)-1,10-phenanthroline). EA calcd for C<sub>37</sub>H<sub>28</sub>N<sub>4</sub>O<sub>2</sub> (%): C 79.27, H 5.03, N 9.99; found: C 79.21, H 5.07, N 10.32. <sup>1</sup>H NMR (500 MHz, CDCl<sub>3</sub>, 298 K): 9.24 (dd,  $J = 4.3, 1.7$  Hz, 1H, H1), 8.74 (dd,  $J = 7.5, 0.5$  Hz, 1H, H8), 8.62 (d,  $J = 8.4$  Hz, 1H, H6), 8.31 (d,  $J = 8.4$  Hz, 1H, H7), 8.27 (dd,  $J = 8.0, 1.7$  Hz, 1H, H3), 7.89 (t,  $J = 7.8$  Hz, 1H, H9), 7.83 (d,  $J = 8.8$  Hz, 1H, H5), 7.79 (d,  $J = 8.8$  Hz, 1H, H4), 7.65 (dd,  $J = 8.0, 4.3$  Hz, 1H, H2), 7.14–7.06 (m, 8H, H11, H12, anisyl-H13, tolyl-H13), 7.01 (d,  $J = 8.5$  Hz, 2H, tolyl-H14), 6.93 (dd,  $J = 8.1, 0.6$  Hz, 1H, H10), 6.86 (d,  $J = 9.0$  Hz, 2H, anisyl-H14), 3.81 (s, 3H, OMe-H15), 2.31 (s, 3H, Me-H15) ppm. <sup>13</sup>C NMR (125.80 MHz, CDCl<sub>3</sub>, 298 K): 163.56, 155.98, 155.86, 154.38, 150.58, 148.78, 146.56, 145.97, 145.81, 145.29, 141.34, 140.50, 137.00, 136.32, 131.83, 129.95, 129.19, 128.98, 126.89, 126.71, 126.69, 123.84, 123.46, 123.06, 122.10, 121.13, 117.31, 114.89, 111.48, 55.65, 20.88 ppm. MS-ESI: 560.2207 ([M], calcd 560.2212).

4-((6-(1,10-Phenanthrolin-2-yl)pyridin-2-yl)oxy)-N,N-bis(4-methoxyphenyl)aniline (**1c**). 750 mg (2.3 mmol) of 4-(bis(4-methoxyphenyl)amino)phenol<sup>79</sup> and 215 mg (1.9 mmol) of potassium *tert*-butoxide were dissolved in 5 mL of anhydrous THF and heated to 60 °C for 2 h. After removing all volatiles under vacuum, 575 mg (1.7 mmol) of 2-(6-bromopyridin-2-yl)-

1,10-phenanthroline were added in a single portion. The reaction mixture was heated to 200 °C overnight. The molten material was cooled down to ambient temperature and dissolved in 40 mL of CH<sub>2</sub>Cl<sub>2</sub> and extracted twice with an aqueous NaHCO<sub>3</sub> solution. The organic phase was dried over Na<sub>2</sub>SO<sub>4</sub> and all volatiles were removed under vacuum. The crude product was purified *via* column chromatography over ALOX (column size: 2.5 × 20 cm) with a mixture of *n*-hexane/CH<sub>2</sub>Cl<sub>2</sub> (1 : 1; v/v) and 3% NEt<sub>3</sub> as the eluent. Yield: 549 mg, yellow solid (56% based on 2-(6-bromopyridin-2-yl)-1,10-phenanthroline). EA calcd for C<sub>37</sub>H<sub>28</sub>N<sub>4</sub>O<sub>3</sub>· $\frac{1}{2}$ H<sub>2</sub>O (%): C 75.98, H 4.85, N 9.59; found: C 75.88, H 4.99, N 9.57. <sup>1</sup>H NMR (500 MHz, CDCl<sub>3</sub>, 298 K): 9.25 (dd, *J* = 4.3, 1.7 Hz, 1H, *H*1), 8.73 (dd, *J* = 7.5, 0.7 Hz, 1H, *H*8), 8.63 (d, *J* = 8.4 Hz, 1H, *H*6), 8.31 (d, *J* = 8.4 Hz, 1H, *H*7), 8.27 (dd, *J* = 8.0, 1.7 Hz, 1H, *H*3), 7.88 (t, *J* = 7.8 Hz, 1H, *H*9), 7.83 (d, *J* = 8.8 Hz, 1H, *H*5), 7.80 (d, *J* = 8.8 Hz, 1H, *H*4), 7.65 (dd, *J* = 8.0, 4.3 Hz, 1H, *H*2), 7.12–7.07 (m, 6H, *H*12, *H*13), 7.04 (d, *J* = 9.0 Hz, 2H, *H*11), 6.92 (dd, *J* = 8.1, 0.7 Hz, 1H, *H*10), 6.85 (d, *J* = 9.0 Hz, 4H, *H*14), 3.80 (s, 6H, *H*15) ppm. <sup>13</sup>C NMR (125.80 MHz, CDCl<sub>3</sub>, 298 K): 163.50, 155.74, 155.59, 154.25, 150.48, 148.16, 146.45, 145.69, 145.54, 141.45, 140.33, 136.86, 136.16, 129.05, 128.84, 126.76, 126.57, 125.94, 122.91, 122.62, 121.92, 120.99, 117.15, 114.72, 111.26, 55.53 ppm. MS-ESI: 576.2156 ([M], calcd 576.2161); 577.2234 ([M + H]<sup>+</sup>, calcd 577.2240); 599.2054 ([M + Na]<sup>+</sup>, calcd 599.2059); 615.1793 ([M + K]<sup>+</sup>, calcd 615.1798).

**General syntheses of complexes [Co(1b,c)<sub>2</sub>](ClO<sub>4</sub>)<sub>2</sub>.** 2 eq. of the appropriate ligand and 1 eq. of cobalt perchlorate hexahydrate were suspended in anhydrous ethanol and were stirred at ambient temperature overnight. The reaction mixture was centrifuged and the precipitate was washed with 2 mL of ethanol and 5 mL of diethyl ether consecutively. The crude product was dissolved in 2 mL of acetonitrile and filtered over Celite. The filtrate was mixed with diethyl ether until a precipitate was formed and centrifuged. The remaining solid was washed with 5 mL of diethyl ether twice and dried under vacuum.

**[Co(1b)<sub>2</sub>](ClO<sub>4</sub>)<sub>2</sub>.** According to the general procedure, 131 mg (0.23 mmol) of **1b** and 43 mg (0.12 mmol) of Co(ClO<sub>4</sub>)<sub>2</sub>·6H<sub>2</sub>O were treated. After appropriate work-up, 138 mg of the title complex could be isolated as a yellow solid (83% based on **1b**). EA calcd for C<sub>74</sub>H<sub>56</sub>Cl<sub>2</sub>CoN<sub>8</sub>O<sub>14</sub>· $\frac{1}{2}$ CH<sub>3</sub>CN (%): C 64.36, H 4.14, N 8.51; found: C 64.24, H 4.16, N 8.57. <sup>1</sup>H NMR (500 MHz, CD<sub>3</sub>CN, 298 K): 171.20 (s, *LW* = 307 Hz, *T*<sub>1</sub> = 2.2 ms, 2H, *H*1), 114.06 (s, *LW* = 62 Hz, *T*<sub>1</sub> = 11.4 Hz, 2H, *H*7), 88.19 (s, *LW* = 45 Hz, *T*<sub>1</sub> = 14 ms, 2H, *H*8), 45.31 (s, *LW* = 16 Hz, *T*<sub>1</sub> = 39 ms, 2H, *H*10), 43.98 (s, *LW* = 18 Hz, *T*<sub>1</sub> = 33 ms, 2H, *H*2), 36.17 (s, *LW* = 15 Hz, *T*<sub>1</sub> = 55 ms, 2H, *H*5), 29.39 (s, *LW* = 19 Hz, *T*<sub>1</sub> = 34 ms, 2H, *H*6), 23.46 (s, *LW* = 12 Hz, *T*<sub>1</sub> = 84 ms, 2H, *H*4), 10.52 (s, *LW* = 12 Hz, *T*<sub>1</sub> = 57 ms, 2H, *H*9), 6.96 (d, *J* = 7.9 Hz, *T*<sub>1</sub> = 889 ms, 4H, tolyl-*H*14), 6.78 (d, *J* = 8.6 Hz, *T*<sub>1</sub> = 857 ms, 4H, anisyl-*H*14), 6.43 (d, *J* = 8.7 Hz, *T*<sub>1</sub> = 411 ms, 4H, anisyl-*H*13), 6.25 (d, *J* = 8.1 Hz, *T*<sub>1</sub> = 401 ms, 4H, tolyl-*H*13), 3.68 (s, *T*<sub>1</sub> = 1.2 s, 6H, OMe-*H*15), 3.16 (s, *LW* = 12 Hz, *T*<sub>1</sub> = 140 ms, 4H, *H*12), 2.15 (s, *T*<sub>1</sub> = 862 ms, 6H, Me-*H*15), −0.96 (s, *LW* = 11 Hz, *T*<sub>1</sub> = 88 ms, 2H, *H*3), −9.87 (s, *LW* = 64 Hz, *T*<sub>1</sub> = 18 ms, 4H, *H*11) ppm. MS-ESI: 1278.3236 ([M − ClO<sub>4</sub>]<sup>+</sup>, calcd 1278.3242).

**[Co(1c)<sub>2</sub>](ClO<sub>4</sub>)<sub>2</sub>.** According to the general procedure, 200 mg (0.35 mmol) of **1c** and 64 mg (0.175 mmol) of Co(ClO<sub>4</sub>)<sub>2</sub>·6H<sub>2</sub>O were treated. After appropriate work-up, 195 mg of the title complex could be isolated as a yellow solid (79% based on **1c**). EA calcd for C<sub>74</sub>H<sub>56</sub>Cl<sub>2</sub>CoN<sub>8</sub>O<sub>14</sub>· $\frac{1}{2}$ CH<sub>3</sub>CN·H<sub>2</sub>O (%): C 61.38, H 4.22, N 8.11; found: C 61.55, 3.89, N 8.13. <sup>1</sup>H NMR (500 MHz, CD<sub>3</sub>CN, 298 K): 171.41 (s, *LW* = 312 Hz, *T*<sub>1</sub> = 4 ms, 2H, *H*1), 114.13 (s, *LW* = 54 Hz, *T*<sub>1</sub> = 11 ms, 2H, *H*7), 88.37 (s, *LW* = 39 Hz, *T*<sub>1</sub> = 13 ms, 2H, *H*8), 45.24 (s, *LW* = 16 Hz, *T*<sub>1</sub> = 37 ms, 2H, *H*10), 43.95 (s, *LW* = 18 Hz, *T*<sub>1</sub> = 31 ms, 2H, *H*2), 36.12 (s, *LW* = 14 Hz, *T*<sub>1</sub> = 53 ms, 2H, *H*5), 29.41 (s, *LW* = 16 Hz, *T*<sub>1</sub> = 32 ms, 2H, *H*6), 23.36 (s, *LW* = 11 Hz, *T*<sub>1</sub> = 80 ms, 2H, *H*4), 10.59 (s, *LW* = 12 Hz, *T*<sub>1</sub> = 53 ms, 2H, *H*9), 6.71 (d, *J* = 8.6 Hz, *T*<sub>1</sub> = 841 ms, 8H, *H*14), 6.37 (d, *J* = 8.7 Hz, *T*<sub>1</sub> = 380 ms, 8H, *H*13), 3.63 (s, *LW* = 5 Hz, *T*<sub>1</sub> = 1.1 s, 12H, *H*15), 3.01 (s, *LW* = 15 Hz, *T*<sub>1</sub> = 132 ms, 4H, *H*12), −1.03 (s, *LW* = 11 Hz, *T*<sub>1</sub> = 74 ms, 2H, *H*3), −10.06 (s, *LW* = 94 Hz, *T*<sub>1</sub> = 17 ms, 4H, *H*11) ppm. <sup>1</sup>H NMR (500 MHz, (CD<sub>3</sub>)<sub>2</sub>CO, 193 K): 295.89 (s, *LW* = 4720 Hz, 2H), 203.12 (s, *LW* = 449 Hz, 2H), 154.64 (s, *LW* = 360 Hz, 2H), 61.24 (s, *LW* = 174 Hz, 2H), 58.93 (s, *LW* = 177 Hz, 2H), 56.93 (s, *LW* = 117 Hz, 2H), 56.33 (s, *LW* = 178 Hz, 2H), 28.82 (s, *LW* = 73 Hz, 2H), 14.21 (s, *LW* = 111 Hz, 2H), 6.22 (s, *LW* = 21 Hz, 8H), 5.50 (s, *LW* = 33 Hz, 8H), 3.18 (s, *LW* = 11 Hz, 12H), −5.36 (s, *LW* = 396 Hz, 4H), −14.75 (s, *LW* = 81 Hz, 2H), −16.56 (s, *LW* = 600 Hz, 4H) ppm. MS-ESI: 1310.3134 ([M − ClO<sub>4</sub>]<sup>+</sup>, calcd 1310.3140).

## Conflicts of interest

There are no conflicts to declare.

## Acknowledgements

This work was financially supported by the Deutsche Forschungsgemeinschaft DFG (PE1513/3-3).

## References

- 1 J.-P. Collin, S. Guillerez, J.-P. Sauvage, F. Barigelletti, L. De Cola, L. Flamigni and V. Balzani, *Inorg. Chem.*, 1991, **30**, 4230–4238.
- 2 K. C. D. Robson, B. D. Koivisto, T. J. Gordon, T. Baumgartner and C. P. Berlinguette, *Inorg. Chem.*, 2010, **49**, 5335–5337.
- 3 C.-J. Yao, R.-H. Zheng, H.-J. Nie, B.-B. Cui, Q. Shi, J. Yao and Y.-W. Zhong, *Chem. – Eur. J.*, 2013, **19**, 12376–12387.
- 4 Y.-M. Zhang, S.-H. Wu, C.-J. Yao, H.-J. Nie and Y.-W. Zhong, *Inorg. Chem.*, 2012, **51**, 11387–11395.
- 5 W. Kaim and B. Sarkar, *Coord. Chem. Rev.*, 2007, **251**, 584–594.
- 6 A. Hildebrandt and H. Lang, *Organometallics*, 2013, **32**, 5640–5653.
- 7 B. S. Brunschwig, C. Creutz and N. Sutin, *Chem. Soc. Rev.*, 2002, **31**, 168–184.

- 8 A. Hildebrandt, D. Miesel and H. Lang, *Coord. Chem. Rev.*, 2018, **371**, 56–66.
- 9 U. Pfaff, A. Hildebrandt, M. Korb, S. Ofswald, M. Linseis, K. Schreiter, S. Spange, R. F. Winter and H. Lang, *Chem. – Eur. J.*, 2016, **22**, 783–801.
- 10 J. M. Speck, M. Korb, A. Schade, S. Spange and H. Lang, *Organometallics*, 2015, **34**, 3788–3798.
- 11 A. Heckmann and C. Lambert, *Angew. Chem., Int. Ed.*, 2012, **51**, 326–392.
- 12 J. Zhang, G. Liu, X.-Y. Wang, G.-A. Yu, J. Yin and S.-H. Liu, *Dyes Pigm.*, 2017, **143**, 416–426.
- 13 O. Sato, *Proc. Jpn. Acad., Ser. B*, 2012, **88**, 213–225.
- 14 O. Sato, J. Tao and Y.-Z. Zhang, *Angew. Chem., Int. Ed.*, 2007, **46**, 2152–2187.
- 15 C. L. Ramirez, C. N. Pegoraro, O. Filevich, A. Bruttomeso, R. Etchenique and A. R. Parise, *Inorg. Chem.*, 2012, **51**, 1261–1268.
- 16 H.-J. Nie, C.-J. Yao, M.-J. Sun, Y.-W. Zhong and J. Yao, *Organometallics*, 2014, **33**, 6223–6231.
- 17 S. Handa, H. Wietasch, M. Thelakkat, J. R. Durrant and S. A. Haque, *Chem. Commun.*, 2007, 1725–1727.
- 18 C. J. Yao, Y. W. Zhong and J. Yao, *Inorg. Chem.*, 2013, **52**, 10000–10008.
- 19 H.-J. Nie, X. Chen, C.-J. Yao, Y.-W. Zhong, G. R. Hutchison and J. Yao, *Chem. – Eur. J.*, 2012, **18**, 14497–14509.
- 20 P. Bonhote, J.-E. Moser, R. Humphry-Baker, N. Vlachopoulos, S. M. Zakeeruddin, L. Walder and M. Grätzel, *J. Am. Chem. Soc.*, 1999, **121**, 1324–1336.
- 21 J. Shen, J. Shao, Z. Gong and Y. Zhong, *Inorg. Chem.*, 2015, **54**, 10776–10784.
- 22 H.-J. Nie, J.-Y. Shao, C.-J. Yao and Y.-W. Zhong, *Chem. Commun.*, 2014, **50**, 10082–10085.
- 23 J. Hankache, M. Niemi, H. Lemmetyinen and O. S. Wenger, *Inorg. Chem.*, 2012, **51**, 6333–6344.
- 24 J. Hankache, M. Niemi, H. Lemmetyinen and O. S. Wenger, *J. Phys. Chem. A*, 2012, **116**, 8159–8168.
- 25 W. Goodall and J. A. G. Williams, *Chem. Commun.*, 2001, 2514–2515.
- 26 S.-H. Hwang, C. N. Moorefield, P. Wang, F. R. Fronczek, B. H. Courtney and G. R. Newkome, *Dalton Trans.*, 2006, 3518–3522.
- 27 T. Jiang, N. Lu, Y. Hang, J. Yang, J. Mei, J. Wang, J. Hua and H. Tian, *J. Mater. Chem. C*, 2016, **4**, 10040–10046.
- 28 X. Bi and Y. Pang, *J. Phys. Chem. B*, 2016, **120**, 3311–3317.
- 29 T. Yu, V. K.-M. Au, D. P.-K. Tsang, M.-Y. Chan and V. W.-W. Yam, *Dalton Trans.*, 2015, **44**, 18983–18992.
- 30 J.-H. Tang, T.-G. Sun, J.-Y. Shao, Z.-L. Gong and Y.-W. Zhong, *Chem. Commun.*, 2017, **53**, 11925–11928.
- 31 K. A. Walters, Y.-J. Kim and J. T. Hupp, *J. Electroanal. Chem.*, 2003, **554–555**, 449–458.
- 32 M.-K. Leung, M.-Y. Chou, Y. O. Su, C. L. Chiang, H.-L. Chen, C. F. Yang, C.-C. Yang, C.-C. Lin and H.-T. Chen, *Org. Lett.*, 2003, **5**, 839–842.
- 33 C.-J. Yao, Y.-W. Zhong and J. Yao, *Inorg. Chem.*, 2013, **52**, 4040–4045.
- 34 J. W. Turner and F. A. Schultz, *Coord. Chem. Rev.*, 2001, **219–221**, 81–97.
- 35 E. Buhks, M. Bixon, J. Jortner and G. Navon, *Inorg. Chem.*, 1979, **18**, 2014–2018.
- 36 S. Larsson, K. Stahl and M. C. Zerner, *Inorg. Chem.*, 1986, **25**, 3033–3037.
- 37 M. D. Newton, *J. Phys. Chem.*, 1991, **95**, 30–38.
- 38 D. Li, R. Clérac, O. Roubeau, E. Harté, C. Mathonière, R. Le Bris and S. M. Holmes, *J. Am. Chem. Soc.*, 2008, **130**, 252–258.
- 39 D. Aguilà, Y. Prado, E. S. Koumoussi, C. Mathonière and R. Clérac, *Chem. Soc. Rev.*, 2016, **45**, 203–224.
- 40 O. Sato and A. Cui, *Acc. Chem. Res.*, 2007, **40**, 361–369.
- 41 T. Tezgerevska, K. G. Alley and C. Boskovic, *Coord. Chem. Rev.*, 2014, **268**, 23–40.
- 42 C. G. Buchanan and R. M. Pierpont, *J. Am. Chem. Soc.*, 1980, **102**, 4951–4957.
- 43 E. Evangelio and D. Ruiz-Molina, *C. R. Chim.*, 2008, **11**, 1137–1154.
- 44 D. Aguilà, Y. Prado, E. S. Koumoussi, C. Mathonière and R. Clérac, *Chem. Soc. Rev.*, 2016, **45**, 203–224.
- 45 L. Schnaubelt, H. Petzold, J. M. Speck, E. Dmitrieva, M. Rosenkranz and M. Korb, *Dalton Trans.*, 2017, **46**, 2690–2698.
- 46 I. Ratera, C. Sporer, D. Ruiz-Molina, N. Ventosa, J. Baggerman, A. M. Brouwer, C. Rovira and J. Veciana, *J. Am. Chem. Soc.*, 2007, **129**, 6117–6129.
- 47 M. Nihei, Y. Sekine, N. Suganami, K. Nakazawa, A. Nakao, H. Nakao, Y. Murakami and H. Oshio, *J. Am. Chem. Soc.*, 2011, **133**, 3592–3600.
- 48 I.-R. Jeon, S. Calancea, A. Panja, D. M. Piñero Cruz, E. S. Koumoussi, P. Dechambenoit, C. Coulon, A. Wattiaux, P. Rosa, C. Mathonière and R. Clérac, *Chem. Sci.*, 2013, **4**, 2463.
- 49 S. Amthor, B. Noller and C. Lambert, *Chem. Phys.*, 2005, **316**, 141–152.
- 50 K. Izutsu, *Electrochemistry in Nonaqueous Solutions*, Wiley-VCH Verlag GmbH & Co. KGaA, 2002.
- 51 H. Petzold, P. Djomgoue, G. Hörner, S. Heider, C. Lochenie, B. Weber, T. Rüffer and D. Schaarschmidt, *Dalton Trans.*, 2017, **46**, 6218–6229.
- 52 H. Petzold, P. Djomgoue, G. Hörner, C. Lochenie, B. Weber and T. Rüffer, *Dalton Trans.*, 2018, **47**, 491–506.
- 53 E. C. Constable, K. Harris, C. E. Housecroft, M. Neuburger and J. A. Zampese, *CrystEngComm*, 2010, **12**, 2949–2961.
- 54 R. S. Gaddie, C. B. Moss and C. M. Elliott, *Langmuir*, 2013, **29**, 825–831.
- 55 R. J. LeSuer, C. Buttolph and W. I. Geiger, *Anal. Chem.*, 2004, **76**, 6395–6401.
- 56 F. Barrière and W. E. Geiger, *J. Am. Chem. Soc.*, 2006, **128**, 3980–3989.
- 57 G. Gritzner and J. Kuta, *Pure Appl. Chem.*, 1984, **56**, 461–466.
- 58 M. J. Plater and T. Jackson, *Tetrahedron*, 2003, **59**, 4673–4685.

- 59 S. Barlow, C. Risko, S.-J. Chung, N. M. Tucker, V. Coropceanu, S. C. Jones, Z. Levi, J.-L. Bre and S. R. Marder, *J. Am. Chem. Soc.*, 2005, **127**, 16900–16911.
- 60 F. Ghamouss, R. Pitson, F. Odobel, M. Boujtita, S. Caramori and C. A. Bignozzi, *Electrochim. Acta*, 2010, **55**, 6517–6522.
- 61 S. Dapperheld, E. Steckhan, K.-H. Grosse Brinkhaus and T. Esch, *Chem. Ber.*, 1991, **124**, 2557–2567.
- 62 U. S. Schubert, C. Eschbaumer, P. Andres, H. Hofmeier, C. H. Weidl, E. Herdtweck, E. Dulkeith, A. Morteani, N. E. Hecker and J. Feldmann, *Synth. Met.*, 2001, **121**, 1249–1252.
- 63 J. K. Klosterman, A. Linden, D. K. Frantz and J. S. Siegel, *Dalton Trans.*, 2010, **39**, 1519–1531.
- 64 J. J. Moore, J. J. Nash, P. E. Fanwick and D. R. Mcmillin, *Inorg. Chem.*, 2002, **41**, 6387–6396.
- 65 M. Krejcek, M. Danek and F. Hartl, *J. Electroanal. Chem.*, 1991, **317**, 179–187.
- 66 C. Mathonière, *Eur. J. Inorg. Chem.*, 2018, **2018**, 248–258.
- 67 B. S. Brunshwig, C. Creutz, D. H. Macartney, T.-K. Sham and N. Sutin, *Faraday Discuss. Chem. Soc.*, 1982, **74**, 113–127.
- 68 M. A. Halcrow, *Chem. Soc. Rev.*, 2011, **40**, 4119–4142.
- 69 E. König, G. Ritter and S. K. Kulshreshtha, *Chem. Rev.*, 1985, **85**, 219–234.
- 70 P. Gütllich, Y. Garcia and H. A. Goodwin, *Chem. Soc. Rev.*, 2000, **29**, 419–427.
- 71 P. Gütllich, A. Hauser and H. Spiering, *Angew. Chem., Int. Ed. Engl.*, 1994, **33**, 2024–2054.
- 72 N. I. Neuman, E. Winkler, O. Pena, M. C. G. Passeggi, A. C. Rizzi and C. D. Brondino, *Inorg. Chem.*, 2014, **53**, 2535–2544.
- 73 J. A. Weil and J. R. Bolton, in *Electron Paramagnetic Resonance*, John Wiley & Sons, Inc., 2006, pp. 301–356.
- 74 F. A. Neugebauer, S. Bamberger and W. R. Groh, *Chem. Ber.*, 1975, **108**, 2406–2415.
- 75 M. Abe, *Chem. Rev.*, 2013, **113**, 7011–7088.
- 76 Y. Su, X. Wang, X. Zheng, Z. Zhang, Y. Song, Y. Sui, Y. Li and X. Wang, *Angew. Chem., Int. Ed.*, 2014, **53**, 2857–2861.
- 77 S. K. Sheppard, G. R. Eaton and S. S. Eaton, *J. Magn. Reson.*, 1985, **63**, 74–87.
- 78 S. S. Eaton and G. R. Eaton, *Coord. Chem. Rev.*, 1988, **83**, 29–72.
- 79 Y. Li and T. Michinobu, *J. Polym. Sci., Part A: Polym. Chem.*, 2012, **50**, 2111–2120.